

# VR-Splatting: Foveated Radiance Field Rendering via 3D Gaussian Splatting and Neural Points

Linus Franke

Laura Fink

Marc Stamminger

{firstname.lastname}@fau.de  
Visual Computing Erlangen  
Friedrich-Alexander-Universität Erlangen-Nürnberg

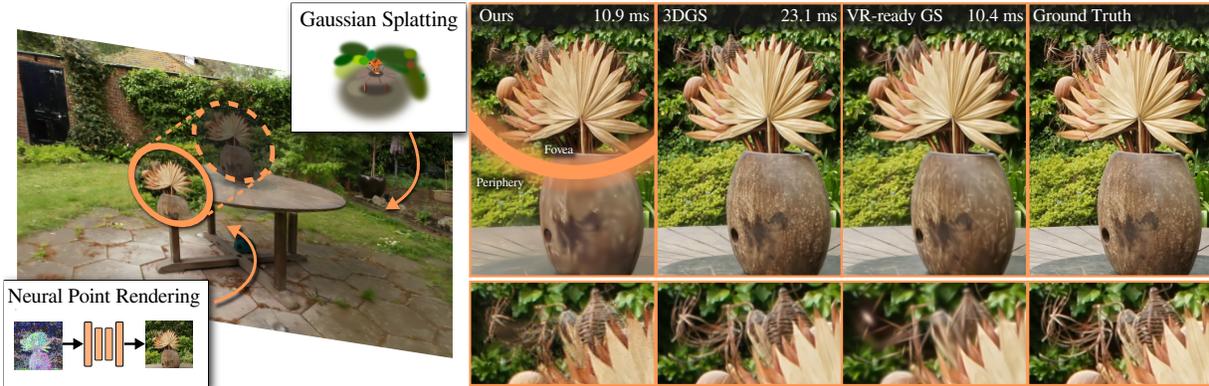


Figure 1: VR-Splatting combines advantages of neural point rendering [23] and 3D Gaussian splatting (3DGS) [43] within a hybrid foveated radiance field rendering system for VR. In contrast to 3DGS and a VR-ready variant, which only uses 0.5 Mio. primitives (see Fig. 2), our method provides high fidelity in the foveal region and meets the 90 Hz VR framerate requirements.

## ABSTRACT

Recent advances in novel view synthesis (NVS), particularly neural radiance fields (NeRF) and Gaussian splatting (3DGS), have demonstrated impressive results in photorealistic scene rendering. These techniques hold great potential for applications in virtual tourism and teleportation, where immersive realism is crucial. However, the high-performance demands of virtual reality (VR) systems present challenges in directly utilizing even such fast-to-render scene representations like 3DGS due to latency and computational constraints.

In this paper, we propose foveated rendering as a promising solution to these obstacles. We analyze state-of-the-art NVS methods with respect to their rendering performance and compatibility with the human visual system. Our approach introduces a novel foveated rendering approach for Virtual Reality, that leverages the sharp, detailed output of neural point rendering for the foveal region, fused with a smooth rendering of 3DGS for the peripheral vision.

Our evaluation confirms that perceived sharpness and detail-richness are increased by our approach compared to a standard VR-ready 3DGS configuration. Our system meets the necessary performance requirements for real-time VR interactions, ultimately enhancing the user’s immersive experience.

Project page: [https://lfranke.github.io/vr\\_splatting](https://lfranke.github.io/vr_splatting)

**Index Terms:** Virtual Reality, Foveated Rendering, Novel View Synthesis, Gaussian Splatting, Neural Rendering

## 1 INTRODUCTION

Virtual teleportation into real-world environments, displayed on a virtual reality (VR) headset is a long standing goal in computer

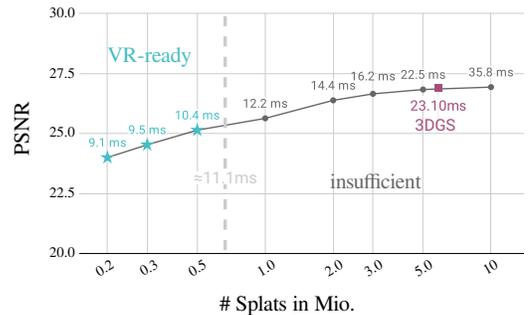


Figure 2: Quality and performance for 3D Gaussian splatting [43]. In the driver recommended settings for the HTC Vive Pro (2468 × 2740 pixels per eye, framerate 90Hz≈11.1ms), the number of Gaussians need to be kept very low, impacting quality (GARDEN half res. dataset). Renderings for 3DGS and 0.5M can be seen in Fig. 1.

graphics and computer vision. State-of-the-art VR headsets exhibit very high resolution displays, which places very high and strict performance demands on rendering algorithms.

In light of this, we propose a novel method that allows for virtual teleportation by exploiting the visual acuity falloff in the periphery via *foveated rendering*. Most foveated rendering algorithms render the foveal region as sharp and crisp as possible while trying to cut computational costs in the periphery by lowering the resolution [29], the number of rays traced [102], or similar. Yet, the application of such techniques is non-trivial as they cause side effects like temporal instability or flickering, which the peripheral vision is highly sensitive to [103].

Recently, 3D Gaussian Splatting [43] emerged as volumetric scene representation for realistic and fast novel view synthesis. Its volumetric nature inherently produces smooth renderings, which

perfectly harmonize with the demands of the peripheral vision. But to achieve pleasing results with crisp details in the foveal region, the required amount of Gaussian primitives pushes the frame times above acceptable levels for VR, as shown in Figs. 1 and 2.

In this paper, we examine the suitability of state-of-the-art novel view synthesis methods for foveated rendering in terms of their compatibility with the human visual system and VR performance requirements, aiming for a smoothly running and visually pleasing VR experience. Instead of a purely 3DGS-based method, that cuts down the number of primitives in the periphery, we opted for a hybrid approach that marries the individual advantages of the chosen methods regarding foveal and periphery reconstruction. In particular, we choose neural point rendering (TRIPS [23]) for the foveal region. Neural point rendering uses neural networks as intelligent image filters that interpret colors from rasterized neural point descriptors and fill holes from projected pixel-sized point clouds. Their tendency to flickering (like ADOP [79]) and especially their drastic performance impact for high resolution output makes them infeasible for full image generation, yet they are a good choice to yield sharp and detail-rich results for the much smaller foveal region.

In this paper, we first discuss necessities for VR radiance field rendering as well as important cues to seamlessly blend different methods together. In that, we arrive at our method, which renders low-detailed Gaussians for the periphery. We apply strong regularization and correct sorting, which yields temporally stable and smooth results. We augment this with neural foveal point rendering for crisp details and apply an edge-based blending function before submitting to an HMD. We contribute:

- A high-fidelity, 90Hz capable technique using foveated rendering of radiance fields for first-person VR rendering.
- The combination of neural point rendering and Gaussian rendering techniques for crisp foveal and smooth peripheral rendering.
- A discussion of requirements for VR-ready splat-based radiance field rendering.
- An evaluation of our foveated rendering method, including a user study showing its effectiveness.

## 2 RELATED WORKS

### 2.1 Foveated Rendering

Exploiting the limitations of the human visual system (HVS) is a well established approach to relax rendering constraints and reduce computational demands [99, 103].

**The Human Visual System.** A key weakness is the decreased visual acuity in the peripheral vision, which foveated rendering techniques leverage. Weier et al. [103] provide a comprehensive overview of the HVS and its exploitable limitations.

For designing rendering algorithms, the retina’s physiology is crucial. The retina contains cones and rods, which respond to light stimuli. Cones, mainly concentrated in the fovea (less than  $10^\circ$  of the visual field), are responsible for sharp, color vision [27]. Rods, in contrast, are motion-sensitive and less color sensitive, dominating the peripheral retina with the highest concentration around  $17^\circ$  from the gaze direction [15]. This distribution allows the human visual field to be modeled with a foveal region (*fovea*) for sharp vision and a peripheral region (*periphery*) sensitive primarily to brightness and motion. Using this model to accelerate rendering is called *foveated rendering*. Sometimes, it is assumed that the users gaze is always centered on the image, then called *fixed foveated rendering*. This assumption, however, can present failure cases and usually requires the foveal region to extend way larger than with eye tracked methods. In our method, we employ eye tracking, as this allows us to keep the foveal region small and achieve better performance.

**Foveated Synthetic Rendering.** The concept of foveated rendering has been extensively investigated in the context of synthetic, artist-created scene rendering [99, 38]. Guenter et al. [29] proposed generating three images per frame with full resolution in the fovea and progressively lower resolution in the periphery, blending them using bilinear upsampling. Nevertheless, this necessitates robust anti-aliasing to mitigate flickering, which can be lessened by decoupling visibility detection from shading [69].

Adaptive sampling in foveated ray tracing [52] also reduces computational load by focusing more samples on the fovea and fewer on the periphery [25, 90, 102, 91]. Stengel et al. [90] use saliency maps to allocate samples effectively, while Weier et al. [102] employ a reprojection scheme to accelerate ray tracing by resampling only problematic areas in the periphery, an idea also transferred to rasterization [21]. Other techniques include log-polar mappings for cost reduction [61, 59], contrast-aware foveation for ray tracing and rasterization [98] and deep foveated reconstruction trained with video [40] or neural super resolution techniques [112].

Further supporting research has explored methods to reduce perceptual artifacts. For instance, adding depth of field [101], developing perceptual image metrics [92, 58, 57], exploring Saliency [88], exploiting eye domination [60], hardware solutions [46] and examining peripheral acuity [34] have all shown promise. Eye-tracking latency requirements [2] suggest that a maximum latency of 50-70 ms is acceptable to avoid artifact noticeability, particularly during rapid eye movements (saccades).

### 2.2 Radiance Field Rendering

Radiance fields are a common set of representations for novel view synthesis (NVS), whereby new views are created from previously unseen angles.

**Traditional Methods.** Traditionally, NVS relied on light fields [28], but image-based rendering, often via warping source views onto geometric proxies [17, 9] has since emerged as a popular alternative [87]. While this rendering can be done very fast and efficiently, quality is highly dependent on the quality of the proxy geometry, although subsequent methods have sought to mitigate these issues [20, 9]. Full 3D reconstructions, which gained traction with the advent of *Structure-from-Motion (SfM)* [89, 81] and *Multi-View Stereo (MVS)* [86, 82, 26], also suffer from similar limitations. While requiring significantly more render time, neural rendering extensions [95] employing learned blending operators [33] and deep learned textures [96] in NVS strongly increase quality.

**Neural Radiance Fields.** More recently, implicit 3D scene representations using volumetric fields have become popular, enabling novel view synthesis through volume rendering without requiring proxy geometry. The *Neural Radiance Field (NeRF)* introduced by Mildenhall et al. [64] has demonstrated remarkable results by encoding entire 3D scenes into a coordinate-based MLP. Subsequent research has addressed challenges related to input view distributions [14, 116, 49, 106], scaling [97, 93, 63] and computation times [5, 66, 11, 14, 65, 94, 7, 6]. Effective strategies include scene space discretization via voxel grids [24], octrees [80, 115], tensor decomposition [10], and faster model inference through neurally textured triangle meshes [13] or mesh baking [111, 74, 75, 19]. Notably, *Instant-NGP* [65] achieved significant improvements in training and rendering speed using a hash grid-based space partitioning scheme, enabling fast training and frame rates up to 10 fps.

**Point-based Radiance Fields.** Compared to NeRFs, point-based radiance fields require an explicit point cloud proxy captured from LiDAR [55], RGB-D cameras with depth fusion [16, 104, 42] or SfM/MVS. Point clouds represent an unstructured set of spatial samples with varying distances between neighbors, closely reflecting the original captured data. Rendering these point clouds is

highly efficient [83, 84, 85], and when augmented with neural descriptors [79, 4, 73, 22, 31, 23, 30, 41] or as proxy for optimized attributes [51, 50], they can produce high-quality images using differentiable point renderers [105, 114] or neural ray-based renderers [108, 67, 1].

A significant issue in point rendering is filling gaps in the rendered images, which has led to the development of two main approaches: *world-space splatting* and *screen-space hole filling* [48]. In world-space splatting, points are rendered as oriented discs or 3D structures, known as "splats" or "surfels," with radii precomputed based on point cloud density. To minimize artifacts, these splats are often combined using Gaussian alpha masks and normalizing blend functions [3, 70, 122]. Recent innovations in this area include optimizing splat sizes [43, 118] and employing neural networks to improve rendering quality [109]. The primary radiance field methodology using splats are *3D Gaussian splatting (3DGS)* [43], which sparked a plethora of subsequent work [12, 107], including algorithmic extensions [117, 35, 45, 72], large-scale variants [76, 44], robotics [62] and dynamic content [56, 110, 37]. These methods are able to render high-quality content at high framerates.

Screen-space hole filling commonly uses small splats at most a few pixels large and fills the resulting sparse image in screen space [4]. Therefore commonly some kind of deep filter is used, either in the form of U-Nets [4], FFT-optimized nets [30, 120] or decoder-only Convolutional Neural Networks [23]. Extensions in this domain include reflection models [50], scene optimization [22, 31, 30, 120], reduced training regimes [32, 73], photometric modeling [79] and linear splat formulations [23, 30].

**VR and Foveated Radiance Field Rendering.** Radiance field rendering methods for VR are sparse, especially due to rendering budget constraints exceeding common methods.

In the domain of NeRFs, FoV-NeRF [18] introduces an egocentric NeRF variant with adapted sampling schemes for foveated rendering. VPRF [100] further this field with a voxel-based representation including a visual sensitivity model. Both inherit challenging inference performance of NeRFs, as the framerate of both stays below 90Hz, limiting free exploration. Similarly, InstantNGP-based super-resolution techniques [54] and variable rate shading approaches [78, 77] achieve impressive results, but still fall short of the framerate and full VR resolution requirements.

Point-based methods also struggle with VR capabilities. Neural point methods like ADOP [79] enable VR rendering, but require low resolutions. Likewise, the recently published official SIBR [8]-based VR implementation as well as Gaussian splatting extensions for Unity and Unreal fail to render high-resolution details due to the amount of Gaussians required. While some methods focus on VR applications [39], they do not prioritize rendering efficiency.

In our method, we present the first method focusing on achieving high fidelity and fast VR rendering of radiance fields.

### 3 REQUIREMENTS FOR NVS IN VR

As discussed in the previous sections, we identify point and splat-based techniques to be promising for fast rendering demands. Additionally, they need to harmonize with the human visual system to provide a decent user experience. With foveated rendering computational resources are optimized, as it aligns with the natural distribution of visual acuity in the eye, ensuring that perceived visual quality remains consistent. The dominance of rod cells in the visual periphery leads to a pronounced flicker sensitivity [69], which is a reoccurring concern in related work [69, 29, 21]. The volumetric nature of 3DGS harmonizes well with this in this context, but providing crisp results for the fovea, while simultaneously meeting performance requirements, is not possible up to now.

Neural point rendering-based methods, like TRIPS, promise sharper results for the same time budgets [23]. Both methods use a

Lagrangian scene representation, but model the splat sizes in different ways: 3DGS models splat size in Euclidian space via variance parameters, while the size of neural points is interpreted in pixel-space using a neural network.

This leads to the fact that also render times scale differently. Neural point rendering methods, like TRIPS, are very sensitive to resolution, while the performance of 3DGS scales with the number of primitives as well as resolution. Tab. 1 illustrates this behavior. Both methods do not meet VR framerate requirements when used with full resolution and their default number of primitives. Simply reducing the number of primitives in case of 3DGS leads to blurry results, as shown in Fig. 1. If, however, only the limited foveal region of the image is rendered in highest quality, both methods become feasible and render in approximately 5 ms, leaving another 5-6 ms budget for the periphery.

We thus opted for a hybrid, foveated renderer, that renders the periphery using 3DGS with a reduced splat count. For the fovea region, we decided to use TRIPS, because it can generate crisper detail in richly textured regions, as shown in Fig. 3. Furthermore, we saw potential to speed up TRIPS in synergy with the 3DGS rendering, which turned out to be the case, as we will show in the results.

		LPIPS PSNR		Resolution		
				Fovea Crop	Full	
# Primitives	Reduced	GS	0.30	25.14	2.8ms	10.4 ms
		TRIPS	0.55	21.69	4.9ms	29.6ms
	Full	GS	0.25	25.69	4.8ms	23.1ms
		TRIPS	0.22	25.39	5.1ms	33.1ms

Table 1: Performance juxtaposition of 3DGS and TRIPS on the GARDEN scene. *Fovea Crop* corresponds to an image crop with a resolution of 512×512 px and *Full* to the recommended VR resolution of 2468×2740 px. LPIPS and PSNR were computed on the evaluation images in native resolution. The *Full* primitive count was 5.8 million for GS and 7.8 million for TRIPS, resulting from the default configurations of the original methods. For *Reduced*, 0.5M primitives were set for both methods.

## 4 METHOD

As input, we use a set of captured real-world images, e.g. from a smartphone or DSLR camera. For our method, we use SfM/MVS [81, 82] to obtain camera intrinsics, poses and point clouds. We first implemented and studied a prototype (Sec. 4.1). This is then refined with more sophisticated peripheral (Sec. 4.2), accelerated foveal rendering (Sec. 4.3), with a fovea and edge-based combination function (Sec. 4.4) optimized from input images (Sec. 4.5). Our full pipeline can be seen in Fig. 5.

### 4.1 First Prototype

We implemented our idea in a first non-optimized prototype and examined the feasibility of our idea in a pilot study. We describe the prototype and the outcomes of this study in this section. In the succeeding sections, we continue with the description of our optimized system, implementing the features derived from the findings of the study.

**Method Prototype.** To render a view in our prototype, we render the point cloud in a foveated fashion, using fixation point information obtained from an HMD’s eye tracker.

For peripheral reconstruction, we use 3D Gaussian splatting. Each splat has an opacity  $\alpha$  and color  $C$ . Their 3D orientation and scaling is parameterized per point via a covariance matrix  $\Sigma$ . These primitives are projected and blended to screen, resulting in a full-resolution image  $G$ . For the study, the splats were initialized from SfM and densified during training, resulting in 0.4M. primitives.



Figure 3: Equal render time comparison for components in our method. Fovea sized crops highlighted. For fine details, TRIPS often shows crisper results.

For the foveal region, we employ TRIPS [23] initialized with a dense point cloud from MVS. Each point has contribution size  $s$  and a compressed neural feature  $\tau$ . The features essentially represent colors, however their higher dimensionality allow more details to be represented. The points are projected and blended to a multi-resolution image pyramid, based on the projected  $s$  [23] and then combined with a small convolutional neural network, resulting in a fovea-sized image  $N$ . For the study,  $G$  and  $N$  were combined with a naive smooth step blending.

The system is trained end-to-end in its hybrid form. Parameters of Gaussians and neural points are optimized via gradient descent from the input images.

**Pilot Study.** To better understand the qualitative requirements of our system, we asked four computer graphics experts (aged 23-28, 1 female, 3 male) with VR-experience for their observations and ratings on a VR-ready 3DGS version (VRGS) (with 0.5M primitives) and contrasted it with our prototype on the popular GARDEN scene from the MipNeRF-360 dataset [6].

The experts were asked to state their most important visual observations. Consistent for both variants, participants noticed distracting popping artifacts, caused by inaccurate depth sorting in 3DGS, as also noted by Radl and Steiner et al. [72]. An example is shown in Fig. 4. The effect is amplified for the user by magnification of the HMD’s lenses and the reduced number of primitives.

Regarding VRGS, participants noted blurred sploches due to underreconstruction with the reduced number of Gaussians [113]. Some also pointed out more blurriness in comparison with our first prototype, which coincides with other work’s observations [23, 30].

For our prototype, the quality of the visual experience was rated slightly lower compared to VRGS. While some mentioned increased detail richness, the experience was overshadowed by artifacts, caused by the naive nature of the implementation. Several things were mentioned: mismatching color palettes as the VGG-loss used for neural point rendering is known to not force color fidelity [121]. Furthermore, suboptimal response of the eye-tracking due to delays and blinking was criticized. Lastly, noise and temporal jittering was mentioned, also noted in related work [79, 4].

The study confirmed that the performance cuts of the VR-ready

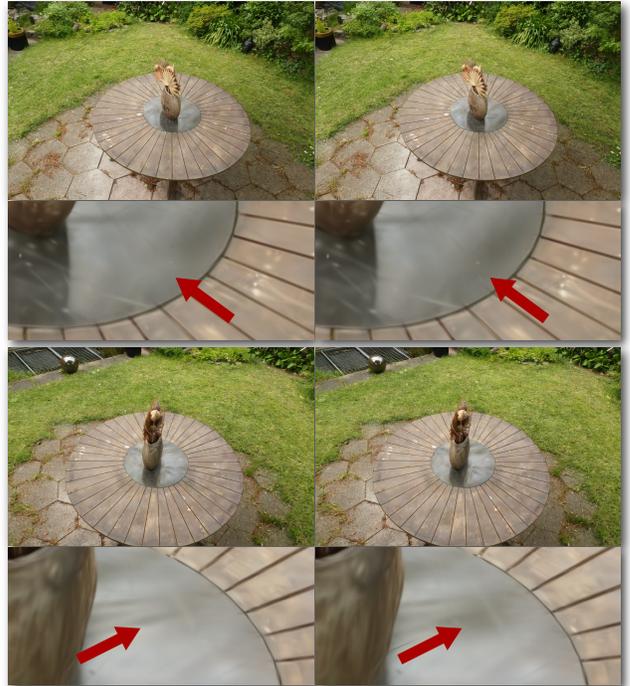


Figure 4: Gaussians in 3DGS "popping" in and out with very small camera movements. This popping is especially noticable in VR, as noted in our pilot study.

version of Gaussian splatting lead to apparent artifacts due to underreconstruction. While the experience of the prototype did not convince off the cuff, it was rated at a similar quality level. However, the experts’ critique proofed that combining peripheral and foveal region is non-trivial and a more sophisticated prototype should aim to mitigate distractions.

Based on these findings, we improve the prototype in three ways: Smoother Gaussian reconstruction for peripheral regions, without popping artifacts (Sec. 4.2), fast foveal reconstruction with well integrated eye-tracking (Sec. 4.3) and a coherent mixture of the models including a matching color palette and subtle blending of high frequency details (Secs. 4.4 and 4.5).

## 4.2 Peripheral Rendering

We identify three main challenges which are required for our Gaussian-based peripheral reconstruction: (1) High rendering performance, (2) little-to-no popping artifacts and (3) little underreconstruction. Usually, these three are conflicting goals, thus we need to carefully design an acceptable solution for all three.

Regarding (2), we adapt the sorting scheme of Radl and Steiner et al. [72], which eliminates popping by hierarchically sorting Gaussian contributions per pixel (instead of per primitive) at the cost of processing time per Gaussian. Similarly, by employing a more finely detailed Gaussian densification heuristic [44, 113], we reduce the severance of (3).

Regarding performance, we need to limit the amount of Gaussians severely (as seen in Tab. 2), which we achieve with regularizing the amount of Gaussians during training (see Sec. 5).

This Gaussian renderer is temporally stable and without severe underreconstruction artifacts. An example rendering can be seen in Fig. 6 (a). Furthermore, we output an approximate depth buffer [72]

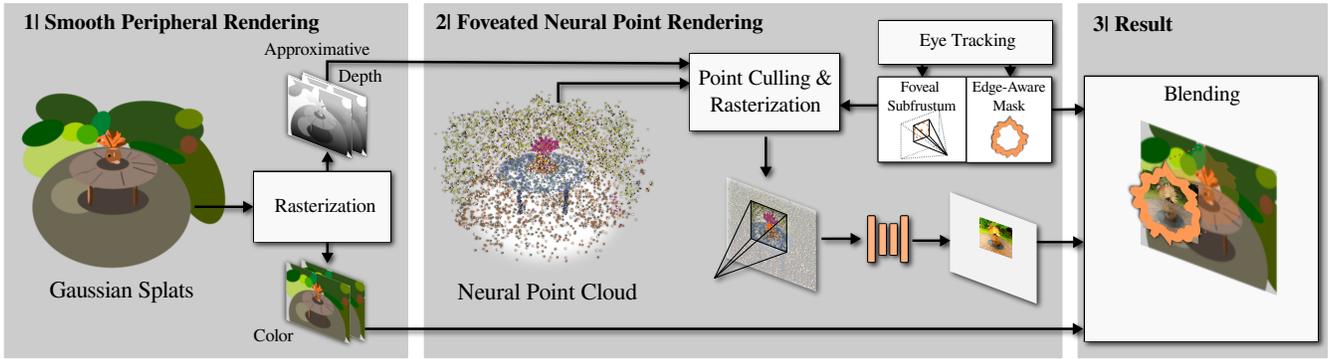


Figure 5: Our Pipeline. A smooth color image and approximate depth map are rendered from a limited set of 3D Gaussians with a temporally stable sorting active (see Section 4.2). Afterwards the eye tracking system is queried to construct a subfrustum via an adapted projection matrix covering only the foveal region. We project a separate neural point cloud with the adapted matrix. Points, occluded by the denser Gaussian splats, are culled against the approximate depth maps and the result is interpreted by a shallow convolutional neural network (see Section 4.3). Eventually, we blend the peripheral color output and the foveal region using an edge-aware mask (see Section 4.4).

by accumulating depths with

$$d = \sum_{i=1}^n d_i \alpha_i \prod_{m=1}^{i-1} (1 - \alpha_m) \quad (1)$$

which is used to accelerate rendering for the foveal reconstruction. Note that we do not mask out the foveal region in this step, but generate a full image. In the following foveal rendering step, we can benefit from this additional information.

### 4.3 Foveal Rendering

For foveal rendering, we revisit TRIPS [23] for this: TRIPS renders points as trilinear splats into an image pyramid and then uses a very small neural network for post-processing. Firstly, this neural network resolves RGB colors from the higher-dimensional neural features, which compress detailed photometric information. The second important task of the neural network is to fill holes in the sparse point cloud renderings.

In our context of foveated rendering, we can improve this pipeline significantly by using the less detailed Gaussian output in the foveal region from the peripheral rendering pass. Firstly, we only render a sub-frustum of the entire scene and discard points outside this frustum early. The sub-frustum is constructed around the fixation point, which is queried after the periphery rendered.

Additionally, we use the approximated depth buffer rendered from the Gaussians to discard occluded points, using a conservative formulation, defined in Eq. 1. This occlusion culling reduces render times and accelerates convergence, as this simplifies visibility evaluation.

Furthermore, we also inject the less detailed rendering from the peripheral rendering pass into the reconstruction network. Thus the network only concentrates on adding fine details, instead of balancing hole filling and crisp reconstruction as in TRIPS. As a side product, this severely lowers training cost, which otherwise would be the bottleneck in this pipeline. Furthermore, experiments showed that we can half the amount of filters for the full resolution layer, further accelerating our pipeline.

### 4.4 Combination

The result of the pipeline are the two images  $G$  (peripheral) and  $N$  (foveal). It is important to be careful when combining both images, as the visual acuity falloff of the human eye is gradual. Therefore, we introduce a combination factor  $c$  including the two terms  $f_p$  (positional) and  $f_e$  (edge-based) for each pixel  $(u, v)$ :



(a) Gaussian Output (b) Combine Mask (c) Our Result

Figure 6: Our combination mask (b) in effect (zoomed in). It is used to adaptively merge Gaussian output with neural point rendering.

$$r_{norm} = \text{clamp} \left( \frac{1}{d_f} \sqrt{(u - e_x)^2 + (v - e_y)^2}, 0, 1 \right) \quad (2)$$

$$f_p = \frac{r_{norm} - m}{1 - m}, \quad (3)$$

with  $e_{x,y}$  being the pixel position of the fixated point,  $d_f$  the fovea radius in pixels and  $m$  the merge interval between 0 and 1. We empirically use  $m = 0.75$  as interval. We set  $d_f$  to 256 pixels, which is larger than the fovea's 7% eccentricity, however necessary due to eye-tracking inaccuracies.

The second factor is the edge factor  $f_e$ , based on the Sobel edge filter  $S$  of the point image  $N$ :

$$f_e = S(N, u, v). \quad (4)$$

Finally,

$$c = 1 - S_2(f_p + \gamma * f_e), \quad (5)$$

using  $\gamma = 0.2$  and with  $S_2$  the smootherstep function  $S_2 = 6x^5 - 15x^4 + 10x^3$  for a smooth transition and well defined derivations. This formulation allows strong edges to extend further in the periphery, so that their change is more gradual.

To account for variance in image exposures, we follow ADOP [79] and use a differentiable camera model to tone-map resulting images to displayable LDR space. This in reverse causes all point features as well as Gaussian color attributes to be stored in HDR-space, and the neural network also outputs HDR float images.

### 4.5 Losses and Optimization

We optimize our pipeline end-to-end. For every iteration, we randomly sample a fixation point and evaluate the pipeline to arrive at

a foveated image. We compare this image to the ground truth and optimize via gradient descent using our loss function  $\mathcal{L}$ :

$$\mathcal{L} = (1 - \lambda) \mathcal{L}_1 + \lambda \mathcal{L}_{D-SSIM} + \mu \mathcal{L}_{VGG}(N) + \beta \mathcal{R} \quad (6)$$

The first two terms are identical to 3DGS [43] with  $\lambda = 0.2$ . We further augment this with the VGG19-loss [53] for neural point rendering with  $\mu = 0.001$ . VGG-loss has proven to work very well for neural point rendering, however for Gaussian Splatting, it increases convergence time and causes artifacts with densification. So we only apply it to the former. Lastly, we introduce a regularizer  $\mathcal{R}$ :

$$\mathcal{R} = |\bar{N} - \overline{F(G)}|, \quad (7)$$

with the foveal cropping function  $F$ . This ensures the mean of  $N$  and the foveal part of  $G$  are similar. This regularizer is vital to remove the color shift, which optimizing with VGG loss otherwise induces. We empirically found  $\beta = 0.00001$ .

We apply a opacity penalty to both Gaussians and neural points opacities [22, 72], which forces the optimization to discard primitives unless absolutely necessary.

## 5 IMPLEMENTATION AND OPTIMIZATION DETAILS

We implemented our method in C++ and CUDA, using torch as the automatic gradient framework and following Patas [68] for a Gaussian Splatting framework and Radl and Steiner et al.’s sorting algorithm [72].

**Training.** For training, we optimize Gaussians for 30000 iterations (as in 3DGS [43]) and neural points for 30000 more iterations, fixing Gaussian parameters during this step. For the first 2000 iterations, both system are trained independently to avoid the faster converging Gaussians to interfere with neural point optimization. Afterwards, gradients from the foveal rendering are also propagated back to Gaussian parameters. Sampling a random eye position every iteration maps very well to cropped training usually employed with convolutional neural networks. After 45000 iterations, we start regularizing the training with  $\mathcal{R}$ .

For densification, we lower thresholds to the original 3DGS and use 0.0002 as densification gradient threshold, 200 as densification interval, 0.005 as opacity threshold and 0.999 as opacity decay every 50 epochs [72]. On our tested scenes, this results in 0.3M to 0.5M Gaussians. On neural points, we impose a gradient penalty of  $10^{-8}$  every update step [22], usually resulting in about 5M points.

**Inference.** For inference, we adapted several aspects to VR rendering. We target the HTC Vive Pro Eye, having an eye-tracker capable update rates of 120Hz. We bake all rendering attributes directly into the point cloud, such as opacities, features and covariances to minimize runtime costs. Furthermore, we defer eye tracking updates until after rendering  $G$ , drastically reducing lag. Also, we output and evaluate all rendering with half float precision and evaluate the network with images for both eyes batched together and accelerated with cuDNN.

For neural point rendering, rendering only the foveal regions allows algorithm performance to be optimized: TRIPS originally renders up to eight progressively lower layers individually, first by counting pixel contributor, then scanning and allocating a buffer for splatting. Starting these many steps introduces overhead, which we can reduce by combining all layer computations into one. This requires about four times the GPU memory, however this rendering is employed on the fovea only. Furthermore, this speeds up computations by about 2ms.

## 6 EVALUATION

To evaluate our method, we chose the popular MipNeRF-360 dataset [6] as well as the INTERMEDIATE set from Tanks&Temples [47]. We compare our method with VRGS, our

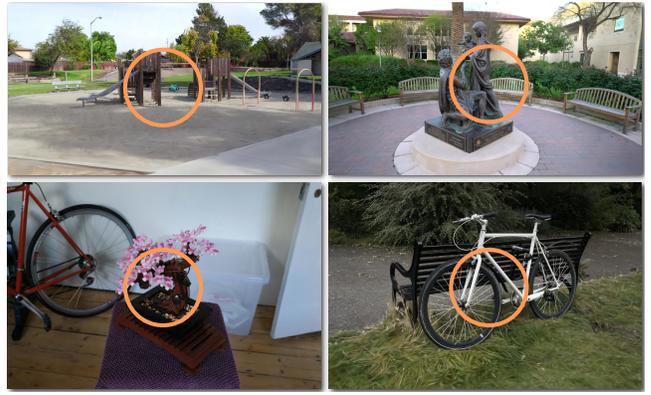


Figure 7: Example renderings of the PLAYGROUND, FAMILY (upper row), BONSAI, and BICYCLE (lower row) scenes used in the user study.

interpretation of a VR-ready version of Gaussian Splatting. Furthermore, we evaluate metrics with 3DGS [43] and TRIPS [23] as qualitative baselines.

### 6.1 Quantitative Evaluation

For quantitative evaluations refer to Tab. 2, averaged per dataset. We compare with the common quality metrics LPIPS<sub>VGG</sub> [119], PSNR and SSIM. For these metrics, we only evaluate the foveal region and omit the periphery. Our experiments show that our method is preferable on the LPIPS metric, which is more perceptually close to the human visual system [119, 121], while being close in the other metrics.

For computing JOD (Just-Objectable-Difference), we use FovVideoVDP [58], which is a perceptual metric including terms for contrast sensitivity and peripheral vision. JOD is defined between 0 and 10, the higher the better. We use it with the preset for the HTC Vive Pro (having the same display system we use) in the setup: "FovVideoVDP v1.2.0, 13.15 [pix/deg], Lpeak=133.3, Lblack=0.1 [cd/m^2], foveated". We compare individual renderings to ground truth and report the averages in Tab. 2. We can see that our method outperforms VR-GS consistently.

Regarding rendering speeds, our method is able to render in more than the VR required 90Hz and is about  $2\times$  faster than 3DGS and  $3\times$  faster than TRIPS. For training speed, we improve drastically on TRIPS, however both Gaussian splatting variants converge faster as no neural network optimization is required.

### 6.2 User Study

For our user study, we evaluated our system (OURS) in comparison to the VR-ready Gaussian Splatting (VRGS) baseline. In our study design, we follow related Deng et al.’s foveated radiance field user study design and evaluation [18].

**Stimuli.** Each stimulus set comprised VR-ready stereo rendering using both OURS and VRGS methods. The resolution for each image was  $2016 \times 2240$  pixels per eye and seated free exploration was possible. We used the GARDEN, BICYCLE and BONSAI scenes from the MipNeRF-360 dataset [6] as well as the FAMILY and PLAYGROUND scenes from the Tanks&Temples dataset [47]. Example renderings are presented in Fig. 7 as well as the teaser (Fig. 1).

**Setup.** Each participant was seated and equipped with an eye-tracked HTC Vive Pro Eye headset to view the stimuli throughout the experiment. The eye-tracker was calibrated for each participant with the default calibration kit. The users had a keyboard in front of them to switch rendering modes at will as well as to confirm

Modality	Method	Performance	MipNeRF-360				Tanks&Temples				Training Time
			JOD $\uparrow$	LPIPS $\downarrow$	PSNR $\uparrow$	SSIM $\uparrow$	JOD $\uparrow$	LPIPS $\downarrow$	PSNR $\uparrow$	SSIM $\uparrow$	
Desktop	3DGS	23.1 ms	7.90	0.247	<b>27.01</b>	<b>0.804</b>	<b>8.24</b>	0.198	<b>27.15</b>	<b>0.874</b>	0.5h
	TRIPS	33.1 ms	<b>8.06</b>	<b>0.222</b>	25.19	0.761	8.15	<b>0.184</b>	24.70	0.835	2.5h
VR	VR-GS	10.4 ms	7.74	0.286	<i>26.45</i>	<i>0.765</i>	8.11	0.211	<i>26.73</i>	<i>0.854</i>	0.4h
	Ours	10.9 ms	<i>8.02</i>	<i>0.237</i>	26.03	0.755	<i>8.16</i>	<i>0.196</i>	25.97	0.815	1.4h

Table 2: Quantitative metrics. JOD (Just-Objectable-Difference) [58] are computed with *FovVideoVDP* for an HTC Vive Pro in foveated mode for the full images. LPIPS, PSNR and SSIM metrics are evaluated for the foveal regions only.



(a) Ground Truth (b) Ours (0.4M) (c) MCMC (0.5M)

Figure 8: Density strategies. 3DGS-MCMC [45] employ a densification scheme up to an exact number of primitives, however their background reconstruction quality is limited compared to ours.

choices. Participants could switch the rendering mode by pressing the spacebar and confirm their choice with the enter button. In total, twelve users (aged 22 to 30, 4 female, 8 male) participated in the experiment.

**Task.** The task followed a two-alternative forced-choice (2AFC) design. Each trial presented a pair of stimuli generated by OURS and VRGS, with the order of viewpoints and the first displayed mode randomized. A mandatory 0.5-second break, displaying a gray screen, was introduced between conditions to reset visual perception, with the same applied between different scenes.

Each participant completed 20 trials throughout the experiment. Prior to the experiment, participants were briefed, and the device was calibrated. During the study, participants were allowed to take as much time as needed to complete each trial.

**Results.** We observe a significantly higher ratio of participant preferring OURS to VRGS ( $\sim 76\%$  preferred OURS,  $SD=0.196$ ). Binomial testing showed significance with  $p < 0.005$ .

**Discussion.** The high ratio of preference for OURS shows the effectiveness of our method. This is underlined by comments made by the participants, which highlighted higher perceived quality and sharpness of our renderings.

### 6.3 Ablation Studies

#### 6.3.1 Densification Strategy for Gaussian Splatting

Recently, Kheradmand et al. [45] introduced a Markov chain dependent Gaussian splatting densification scheme. It allows to exactly determine the number of Gaussians compared to our heuristic based densification. This method would be preferable, as our densification heuristic has to be kept conservative to avoid overshooting the VR limit.

As shown in Fig. 8, the low amount of primitives result in great foreground reconstruction, however deteriorated backgrounds. This introduces severe artifacts in the peripheral reconstruction, including spiky Gaussians with high color variance unsuitable for smooth peripheral rendering. We thus decided to stick to our heuristic densification strategy.

#### 6.3.2 Performance Ablation

We ablate our rendering performance in Tab. 3, with individual features turned off. About half the render time is spent on foveal and

	GS	Fov-PR	Unet	Combine	Exp.	All
Ours	4.9	3.5	1.6	0.5	0.4	10.9
w/o depth	4.8	4.0	1.6	0.5	0.4	+0.4
w/o smaller net	4.9	3.5	1.9	0.5	0.4	+0.3
w/o opacity penalty	7.2	3.7	1.6	0.5	0.4	+2.5
w/o popping fix	2.6	3.5	1.6	0.5	0.4	-2.3
w/o combine $e$	4.9	3.5	1.6	0.3	0.4	-0.2

Table 3: Performance Ablations of our features and improvements.

peripheral reconstruction (upper part). The enhancements mentioned in Section 4 all measurably improve performance (middle part). Our introduced quality enhancing features (lower parts) have performance impacts, especially the hierarchical sorting approach to fix popping [72].

## 7 LIMITATIONS & FUTURE WORK

We inherit limitations from both Gaussian Splatting [43] and TRIPS [23]. In particular, we require good capturing densities, as otherwise holes or missing areas are present. Furthermore, we are dependent on COLMAP for SfM/MVS results, otherwise artifacts due to miss-calibrations occur. Slight camera pose errors are optimized by our pipeline, however severe errors cannot be compensated.

Our approach as well as the VR Gaussian baseline suffer from floaters, which is furthered by the low densification thresholds used. Passing through floaters can be perceived as flickering and be distracting in VR. Stronger mitigation methods [71, 36] would be beneficial in these cases.

Additionally, study participants commented on the lack of sky in our scenes, limiting realism. Solving this with diffusion or generative models might be a great way to increase immersion.

Our hardware also presents challenges. We had to increase fovea sizes as the eyetracker proved inaccurate during initial experiments. With better calibrated and more accurate gaze position, further performance increases may be possible in our method.

## 8 CONCLUSION

In conclusion, our proposed foveated rendering approach demonstrates a viable solution to overcoming the computational demand of radiance field rendering into real-time virtual reality systems. By blending high-detail neural point rendering for the foveal region with smooth 3DGS rendering for peripheral vision, we have shown that it is possible to render radiance fields crisp and immersive without compromising system performance. Our hybrid solution meets the performance demands of VR interactions, offering a significant improvement in rendering quality and user experience, paving the way for more realistic and immersive VR applications in fields such as virtual tourism and teleportation.

## ACKNOWLEDGMENTS

We thank Matthias Innmann, Stefan Romberg, Michael Gerstmayr and Tim Habigt for the fruitful discussions as well as NavVis GmbH for providing the datasets for testing.

Linus Franke was supported by the Bayerische Forschungsförderung (Bavarian Research Foundation) AZ-1422-20 and the 5G

innovation program of the German Federal Ministry for Digital and Transport under the funding code 165GU103B.

The authors gratefully acknowledge the scientific support and HPC resources provided by the Erlangen National High Performance Computing Center (NHR@FAU) of the Friedrich-Alexander-Universität Erlangen-Nürnberg (FAU) under the NHR project *b162dc*. NHR funding is provided by federal and Bavarian state authorities. NHR@FAU hardware is partially funded by the German Research Foundation (DFG) – 440719683.

## REFERENCES

- [1] J. Abou-Chakra, F. Dayoub, and N. Sünderhauf. Particlenerf: A particle-based encoding for online neural radiance fields. In *Proceedings of the IEEE/CVF Winter Conference on Applications of Computer Vision*, pp. 5975–5984, 2024. 3
- [2] R. Albert, A. Patney, D. Luebke, and J. Kim. Latency Requirements for Foveated Rendering in Virtual Reality. *ACM Transactions on Applied Perception (TAP)*, 14(4):25, 2017. 2
- [3] M. Alexa, M. Gross, M. Pauly, H. Pfister, M. Stamminger, and M. Zwicker. Point-based computer graphics. In *ACM SIGGRAPH 2004 Course Notes*, pp. 7–es, 2004. 3
- [4] K.-A. Aliev, A. Sevastopolsky, M. Kolos, D. Ulyanov, and V. Lempitsky. Neural point-based graphics. In *ECCV*, 2020. doi: 10.1007/978-3-030-58542-6\_42 3, 4
- [5] J. T. Barron, B. Mildenhall, M. Tancik, P. Hedman, R. Martinbrualla, and P. P. Srinivasan. Mip-nerf: A multiscale representation for anti-aliasing neural radiance fields. *ICCV*, 2021. doi: 10.1109/ICCV48922.2021.00580 2
- [6] J. T. Barron, B. Mildenhall, D. Verbin, P. P. Srinivasan, and P. Hedman. Mip-nerf 360: Unbounded anti-aliased neural radiance fields. *CVPR*, 2022. doi: 10.1109/CVPR52688.2022.00539 2, 4, 6
- [7] J. T. Barron, B. Mildenhall, D. Verbin, P. P. Srinivasan, and P. Hedman. Zip-nerf: Anti-aliased grid-based neural radiance fields. In *ICCV*, pp. 19640–19648, October 2023. doi: 10.1109/ICCV51070.2023.01804 2
- [8] S. Bonopera, P. Hedman, J. Esnault, S. Prakash, S. Rodriguez, T. Thonat, M. Benadel, G. Chaurasia, J. Philip, and G. Drettakis. sibr: A system for image based rendering, 2020. 3
- [9] G. Chaurasia, S. Duchene, O. Sorkine-Hornung, and G. Drettakis. Depth synthesis and local warps for plausible image-based navigation. *ACM TOG*, 32(3):1–12, 2013. 2
- [10] A. Chen, Z. Xu, A. Geiger, J. Yu, and H. Su. TensorRF: Tensorial radiance fields. In *ECCV*, 2022. doi: 10.1007/978-3-031-19824-3\_20 2
- [11] A. Chen, Z. Xu, F. Zhao, X. Zhang, F. Xiang, J. Yu, and H. Su. Mvs-nerf: Fast generalizable radiance field reconstruction from multi-view stereo. In *Proceedings of the IEEE/CVF International Conference on Computer Vision*, pp. 14124–14133, 2021. 2
- [12] G. Chen and W. Wang. A survey on 3d gaussian splatting. *arXiv preprint arXiv:2401.03890*, 2024. 3
- [13] Z. Chen, T. Funkhouser, P. Hedman, and A. Tagliasacchi. Mobilenerf: Exploiting the polygon rasterization pipeline for efficient neural field rendering on mobile architectures. In *CVPR*, pp. 16569–16578, 2023. 2
- [14] J. Chibane, A. Bansal, V. Lazova, and G. Pons-Moll. Stereo radiance fields (srf): Learning view synthesis for sparse views of novel scenes. In *CVPR*, pp. 7911–7920, 2021. 2
- [15] C. A. Curcio, K. R. Sloan, R. E. Kalina, and A. E. Hendrickson. Human Photoreceptor Topography. *Journal of Comparative Neurology*, 292(4):497–523, 1990. 2
- [16] A. Dai, M. Nießner, M. Zollhöfer, S. Izadi, and C. Theobalt. Bundlefusion: Real-time globally consistent 3d reconstruction using on-the-fly surface reintegration. *ACM Transactions on Graphics (ToG)*, 36(4):1, 2017. 2
- [17] P. Debevec, Y. Yu, and G. Boshokov. Efficient view-dependent ibr with projective texture-mapping. In *EG Rendering Workshop*, vol. 4, 1998. 2
- [18] N. Deng, Z. He, J. Ye, B. Duinkharjav, P. Chakravarthula, X. Yang, and Q. Sun. Fov-nerf: Foveated neural radiance fields for virtual reality. *IEEE TVCG*, 2022. doi: 10.1109/TVCG.2022.3203102 3, 6
- [19] D. Duckworth, P. Hedman, C. Reiser, P. Zhizhin, J.-F. Thibert, M. Lučić, R. Szeliski, and J. T. Barron. Smerf: Streamable memory efficient radiance fields for real-time large-scene exploration. *arXiv preprint arXiv:2312.07541*, 2023. 2
- [20] M. Eisemann, B. De Decker, M. Magnor, P. Bekaert, E. De Aguiar, N. Ahmed, C. Theobalt, and A. Sellent. Floating textures. In *Comput. Graph. Forum*, vol. 27, pp. 409–418. Wiley Online Library, 2008. 2
- [21] L. Franke, L. Fink, J. Martschinke, K. Selgrad, and M. Stamminger. Time-warped foveated rendering for virtual reality headsets. *Computer Graphics Forum*, 40(1):110–123, 2021. doi: 10.1111/cgf.14176 2, 3
- [22] L. Franke, D. Rückert, L. Fink, M. Innmann, and M. Stamminger. Vet: Visual error tomography for point cloud completion and high-quality neural rendering. In *SIGGRAPH Asia*. Association for Computing Machinery, New York, NY, USA, Dec. 2023. 3, 6
- [23] L. Franke, D. Rückert, L. Fink, and M. Stamminger. Trips: Trilinear point splatting for real-time radiance field rendering. *Comput. Graph. Forum*, 43(2), 2024. doi: 10.1111/cgf.15012 1, 2, 3, 4, 5, 6, 7
- [24] S. Fridovich-Keil, A. Yu, M. Tancik, Q. Chen, B. Recht, and A. Kanazawa. Plenoxels: Radiance fields without neural networks. In *2022 IEEE/CVF Conference on Computer Vision and Pattern Recognition (CVPR)*, pp. 5491–5500, 2022. doi: 10.1109/CVPR52688.2022.00542 2
- [25] S. Friston, T. Ritschel, and A. Steed. Perceptual rasterization for head-mounted display image synthesis. *ACM Transactions on Graphics (TOG)*, 38(4):1–14, 2019. 2
- [26] M. Goesele, N. Snavely, B. Curless, H. Hoppe, and S. M. Seitz. Multi-view stereo for community photo collections. In *2007 IEEE 11th International Conference on Computer Vision*, pp. 1–8. IEEE, 2007. 2
- [27] E. B. Goldstein and J. Brockmole. *Sensation and Perception*. Cengage Learning, 2016. 2
- [28] S. J. Gortler, R. Grzeszczuk, R. Szeliski, and M. F. Cohen. The Lumigraph. In *CGIT*, 1996. doi: 10.1145/237170.237200 2
- [29] B. Guenter, M. Finch, S. Drucker, D. Tan, and J. Snyder. Foveated 3D Graphics. *ACM Transactions on Graphics (TOG)*, 31(6):164, 2012. 1, 2, 3
- [30] F. Hahlbohm, L. Franke, M. Kappel, S. Castillo, M. Stamminger, and M. Magnor. Inpc: Implicit neural point clouds for radiance field rendering. *arXiv preprint arXiv:2403.16862*, 2024. 3, 4
- [31] F. Hahlbohm, M. Kappel, J.-P. Tauscher, M. Eisemann, and M. Magnor. Plenopticpoints: Rasterizing neural feature points for high-quality novel view synthesis. In T. Grosch and M. Guthe, eds., *Proc. Vision, Modeling and Visualization (VMV)*, pp. 53–61. Eurographics, Sep 2023. doi: 10.2312/vmv.20231226 3
- [32] M. Harrer, L. Franke, L. Fink, M. Stamminger, and T. Weyrich. In-ovis: Instant novel-view synthesis. In *SIGGRAPH Asia*. Association for Computing Machinery, New York, NY, USA, Dec. 2023. doi: 10.1145/3610548.3618216 3
- [33] P. Hedman, J. Philip, T. Price, J.-M. Frahm, G. Drettakis, and G. Brostow. Deep blending for free-viewpoint image-based rendering. *ACM TOG*, 37(6):1–15, 2018. 2
- [34] D. Hoffman, Z. Meraz, and E. Turner. Limits of peripheral acuity and implications for vr system design. *Journal of the Society for Information Display*, 26(8):483–495, 2018. 2
- [35] B. Huang, Z. Yu, A. Chen, A. Geiger, and S. Gao. 2d gaussian splatting for geometrically accurate radiance fields. In *SIGGRAPH 2024 Conference Papers*. Association for Computing Machinery, 2024. doi: 10.1145/3641519.3657428 3
- [36] B. Huang, Z. Yu, A. Chen, A. Geiger, and S. Gao. 2d gaussian splatting for geometrically accurate radiance fields. In *SIGGRAPH*, pp. 1–11, 2024. 7
- [37] Y.-H. Huang, Y.-T. Sun, Z. Yang, X. Lyu, Y.-P. Cao, and X. Qi. Scgs: Sparse-controlled gaussian splatting for editable dynamic scenes. *arXiv preprint arXiv:2312.14937*, 2023. 3
- [38] S. Jabbireddy, X. Sun, X. Meng, and A. Varshney. Foveated rendering: Motivation, taxonomy, and research directions. *arXiv preprint arXiv:2205.04529*, 2022. 2

- [39] Y. Jiang, C. Yu, T. Xie, X. Li, Y. Feng, H. Wang, M. Li, H. Lau, F. Gao, Y. Yang, et al. Vr-gs: a physical dynamics-aware interactive gaussian splatting system in virtual reality. In *ACM SIGGRAPH 2024 Conference Papers*, pp. 1–1, 2024. 3
- [40] A. S. Kaplanyan, A. Sochenov, T. Leimkühler, M. Okunev, T. Goodall, and G. Rufo. Deepfovea: Neural reconstruction for foveated rendering and video compression using learned statistics of natural videos. *ACM Transactions on Graphics (TOG)*, 38(6):1–13, 2019. 2
- [41] M. Kappel, F. Hahlbohm, T. Scholz, S. Castillo, C. Theobalt, M. Eisemann, V. Golyanik, and M. Magnor. D-npc: Dynamic neural point clouds for non-rigid view synthesis from monocular video. *arXiv preprint arXiv:2406.10078*, 2024. 3
- [42] M. Keller, D. Lefloch, M. Lambers, S. Izadi, T. Weyrich, and A. Kolb. Real-time 3D reconstruction in dynamic scenes using point-based fusion. In *Proc. of Joint 3DIM/3DPVT Conference (3DV)*, pp. 1–8, June 2013. Selected for oral presentation. 2
- [43] B. Kerbl, G. Kopanas, T. Leimkühler, and G. Drettakis. 3D Gaussian splatting for real-time radiance field rendering. *ACM TOG*, 42(4), July 2023. doi: 10.1145/3592433 1, 3, 4, 6, 7
- [44] B. Kerbl, A. Meuleman, G. Kopanas, M. Wimmer, A. Lanvin, and G. Drettakis. A hierarchical 3d gaussian representation for real-time rendering of very large datasets. *ACM TOG*, 43(4):1–15, 2024. 3, 4
- [45] S. Kheradmand, D. Rebain, G. Sharma, W. Sun, J. Tseng, H. Isack, A. Kar, A. Tagliasacchi, and K. M. Yi. 3d gaussian splatting as markov chain monte carlo. *arXiv preprint arXiv:2404.09591*, 2024. 3, 7
- [46] J. Kim, Y. Jeong, M. Stengel, K. Aksit, R. A. Albert, B. Boudaoud, T. Greer, J. Kim, W. Lopes, Z. Majercik, et al. Foveated ar: dynamically-foveated augmented reality display. *ACM Trans. Graph.*, 38(4):99–1, 2019. 2
- [47] A. Knapitsch, J. Park, Q.-Y. Zhou, and V. Koltun. Tanks and temples: Benchmarking large-scale scene reconstruction. *ACM Transactions on Graphics*, 36(4), 2017. 6
- [48] L. Kobbelt and M. Botsch. A survey of point-based techniques in computer graphics. *Computers & Graphics*, 28(6):801–814, 2004. 3
- [49] G. Kopanas and G. Drettakis. Improving NeRF Quality by Progressive Camera Placement for Free-Viewpoint Navigation. In M. Guthe and T. Grosch, eds., *Vision, Modeling, and Visualization*. The Eurographics Association, 2023. doi: 10.2312/vmv.20231222 2
- [50] G. Kopanas, T. Leimkühler, G. Rainer, C. Jambon, and G. Drettakis. Neural point catacaustics for novel-view synthesis of reflections. *ACM TOG*, 2022. doi: 10.1145/3550454.3555497 3
- [51] G. Kopanas, J. Philip, T. Leimkühler, and G. Drettakis. Point-based neural rendering with per-view optimization. *CGF*, 2021. doi: 10.1111/cgf.14339 3
- [52] M. Koskela, T. Viitanen, P. Jääskeläinen, and J. Takala. Foveated path tracing: a literature review and a performance gain analysis. In *Advances in Visual Computing: 12th International Symposium, ISVC 2016, Las Vegas, NV, USA, December 12-14, 2016, Proceedings, Part I 12*, pp. 723–732. Springer, 2016. 2
- [53] C. Ledig, L. Theis, F. Huszár, J. Caballero, A. Cunningham, A. Acosta, A. Aitken, A. Tejani, J. Totz, Z. Wang, et al. Photo-realistic single image super-resolution using a generative adversarial network. In *CVPR*, pp. 4681–4690, 2017. 6
- [54] K. Li, T. Rolff, S. Schmidt, R. Bacher, S. Frintrop, W. Leemans, and F. Steinicke. Immersive neural graphics primitives. *arXiv preprint arXiv:2211.13494*, 2022. 3
- [55] Y. Liao, J. Xie, and A. Geiger. Kitti-360: A novel dataset and benchmarks for urban scene understanding in 2d and 3d. *IEEE Transactions on Pattern Analysis and Machine Intelligence*, 45(3):3292–3310, 2022. 2
- [56] J. Luiten, G. Kopanas, B. Leibe, and D. Ramanan. Dynamic 3d gaussians: Tracking by persistent dynamic view synthesis. *arXiv preprint arXiv:2308.09713*, 2023. 3
- [57] R. K. Mantiuk, M. Ashraf, and A. Chapiro. stelacsf: A unified model of contrast sensitivity as the function of spatio-temporal frequency, eccentricity, luminance and area. *ACM Transactions on Graphics (TOG)*, 41(4):1–16, 2022. 2
- [58] R. K. Mantiuk, G. Denes, A. Chapiro, A. Kaplanyan, G. Rufo, R. Bachy, T. Lian, and A. Patney. Fovvideovdp: A visible difference predictor for wide field-of-view video. *ACM Transactions on Graphics (TOG)*, 40(4):1–19, 2021. 2, 6, 7
- [59] X. Meng, R. Du, J. F. JaJa, and A. Varshney. 3d-kernel foveated rendering for light fields. *IEEE Transactions on Visualization and Computer Graphics*, 27(8):3350–3360, 2020. 2
- [60] X. Meng, R. Du, and A. Varshney. Eye-dominance-guided foveated rendering. *IEEE transactions on visualization and computer graphics*, 26(5):1972–1980, 2020. 2
- [61] X. Meng, R. Du, M. Zwicker, and A. Varshney. Kernel Foveated Rendering. *Proceedings of the ACM on Computer Graphics and Interactive Techniques*, 1(1):5, 2018. 2
- [62] L. Meyer, F. Erich, Y. Yoshiyasu, M. Stamminger, N. Ando, and Y. Domae. Pegasus: Physically enhanced gaussian splatting simulation system for 6dof object pose dataset generation. *arXiv preprint arXiv:2401.02281*, 2024. 3
- [63] Z. Mi and D. Xu. Switch-nerf: Learning scene decomposition with mixture of experts for large-scale neural radiance fields. In *International Conference on Learning Representations (ICLR)*, 2023. 2
- [64] B. Mildenhall, P. P. Srinivasan, M. Tancik, J. T. Barron, R. Ramamoorthi, and R. Ng. NeRF: Representing scenes as neural radiance fields for view synthesis. In *ECCV*, 2020. doi: 10.1145/3503250 2
- [65] T. Müller, A. Evans, C. Schied, and A. Keller. Instant neural graphics primitives with a multiresolution hash encoding. *ACM TOG*, 41(4), jul 2022. doi: 10.1145/3528223.3530127 2
- [66] T. Neff, P. Stadlbauer, M. Parger, A. Kurz, J. H. Mueller, C. R. A. Chaitanya, A. S. Kaplanyan, and M. Steinberger. DONERF: Towards Real-Time Rendering of Compact Neural Radiance Fields using Depth Oracle Networks. *CGF*, 2021. doi: 10.1111/cgf.14340 2
- [67] J. Ost, I. Laradji, A. Newell, Y. Bahat, and F. Heide. Neural point light fields. In *Proceedings of the IEEE/CVF Conference on Computer Vision and Pattern Recognition*, pp. 18419–18429, 2022. 3
- [68] J. Patas. Gaussian splatting cuda. <https://github.com/MrNeRF/gaussian-splatting-cuda>. 6
- [69] A. Patney, M. Salvi, J. Kim, A. Kaplanyan, C. Wyman, N. Bentley, D. Luebke, and A. Lefohn. Towards Foveated Rendering for Gaze-Tracked Virtual Reality. *ACM Transactions on Graphics (TOG)*, 35(6):179, 2016. 2, 3
- [70] H. Pfister, M. Zwicker, J. Van Baar, and M. Gross. Surfels: Surface elements as rendering primitives. In *Proceedings of the 27th annual conference on Computer graphics and interactive techniques*, pp. 335–342, 2000. 3
- [71] J. Philip and V. Deschaintre. Floaters no more: Radiance field gradient scaling for improved near-camera training. 2023. 7
- [72] L. Radl, M. Steiner, M. Parger, A. Weinrauch, B. Kerbl, and M. Steinberger. Stopthepop: Sorted gaussian splatting for view-consistent real-time rendering. *ACM TOG*, 43(4):1–17, 2024. 3, 4, 6, 7
- [73] R. Rakhimov, A.-T. Ardelean, V. Lempitsky, and E. Burnaev. NPBG++: Accelerating neural point-based graphics. In *CVPR*, 2022. doi: 10.1109/CVPR52688.2022.01550 3
- [74] C. Reiser, S. Garbin, P. P. Srinivasan, D. Verbin, R. Szeliski, B. Mildenhall, J. T. Barron, P. Hedman, and A. Geiger. Binary opacity grids: Capturing fine geometric detail for mesh-based view synthesis. *arXiv preprint arXiv:2402.12377*, 2024. 2
- [75] C. Reiser, R. Szeliski, D. Verbin, P. P. Srinivasan, B. Mildenhall, A. Geiger, J. T. Barron, and P. Hedman. Merf: Memory-efficient radiance fields for real-time view synthesis in unbounded scenes. *SIGGRAPH*, 2023. doi: 10.1145/3592426 2
- [76] K. Ren, L. Jiang, T. Lu, M. Yu, L. Xu, Z. Ni, and B. Dai. Octree-gs: Towards consistent real-time rendering with lod-structured 3d gaussians, 2024. 3
- [77] T. Rolff, K. Li, J. Hertel, S. Schmidt, S. Frintrop, and F. Steinicke. Interactive vrs-nerf: Lightning fast neural radiance field rendering for virtual reality. In *Proceedings of the 2023 ACM Symposium on Spatial User Interaction*, pp. 1–3, 2023. 3
- [78] T. Rolff, S. Schmidt, K. Li, F. Steinicke, and S. Frintrop. Vrs-nerf: Accelerating neural radiance field rendering with variable rate shad-

- ing. In *2023 IEEE International Symposium on Mixed and Augmented Reality (ISMAR)*, pp. 243–252. IEEE, 2023. 3
- [79] D. Rückert, L. Franke, and M. Stamminger. Adop: Approximate differentiable one-pixel point rendering. *ACM TOG*, 2022. doi: 10.1145/3528223.3530122 2, 3, 4, 5
- [80] D. Rückert, Y. Wang, R. Li, R. Idoughi, and W. Heidrich. Neat: Neural adaptive tomography. *ACM Trans. Graph.*, 41(4), jul 2022. doi: 10.1145/3528223.3530121 2
- [81] J. L. Schönberger and J.-M. Frahm. Structure-from-motion revisited. In *CVPR*, pp. 4104–4113, 2016. doi: 10.1109/CVPR.2016.445 2, 3
- [82] J. L. Schönberger, E. Zheng, M. Pollefeys, and J.-M. Frahm. Pixel-wise view selection for unstructured multi-view stereo. In *European Conference on Computer Vision (ECCV)*, 2016. 2, 3
- [83] M. Schütz, B. Kerbl, and M. Wimmer. Rendering point clouds with compute shaders and vertex order optimization. In *Computer Graphics Forum*, vol. 40, pp. 115–126. Wiley Online Library, 2021. 3
- [84] M. Schütz, B. Kerbl, and M. Wimmer. Software rasterization of 2 billion points in real time. *ACM Comput. Graph. Int. Techn.*, 5(3):1–17, 2022. 3
- [85] M. Schütz, K. Krösl, and M. Wimmer. Real-time continuous level of detail rendering of point clouds. In *2019 IEEE Conference on Virtual Reality and 3D User Interfaces (VR)*, pp. 103–110. IEEE, 2019. 3
- [86] S. M. Seitz, B. Curless, J. Diebel, D. Scharstein, and R. Szeliski. A comparison and evaluation of multi-view stereo reconstruction algorithms. In *2006 IEEE computer society conference on computer vision and pattern recognition (CVPR'06)*, vol. 1, pp. 519–528. IEEE, 2006. 2
- [87] H. Shum and S. B. Kang. Review of image-based rendering techniques. In *Visual Communications and Image Processing 2000*, vol. 4067, pp. 2–13. SPIE, 2000. 2
- [88] V. Sitzmann, A. Serrano, A. Pavel, M. Agrawala, D. Gutierrez, B. Masia, and G. Wetzstein. Saliency in VR: How do people explore virtual environments? *IEEE transactions on visualization and computer graphics*, 24(4):1633–1642, 2018. 2
- [89] N. Snavely, S. M. Seitz, and R. Szeliski. Photo tourism: exploring photo collections in 3d. In *ACM Siggraph 2006*, pp. 835–846, 2006. 2
- [90] M. Stengel, S. Grogoric, M. Eisemann, and M. Magnor. Adaptive Image-Space Sampling for Gaze-Contingent Real-Time Rendering. In *Computer Graphics Forum*, vol. 35, pp. 129–139. Wiley Online Library, 2016. 2
- [91] Q. Sun, F.-C. Huang, J. Kim, L.-Y. Wei, D. Luebke, and A. Kaufman. Perceptually-guided foveation for light field displays. *ACM Transactions on Graphics (TOG)*, 36(6):192, 2017. 2
- [92] N. T. Swafford, J. A. Iglesias-Guitian, C. Koniaris, B. Moon, D. Cosker, and K. Mitchell. User, metric, and computational evaluation of foveated rendering methods. In *Proceedings of the ACM Symposium on Applied Perception*, pp. 7–14, 2016. 2
- [93] M. Tancik, V. Casser, X. Yan, S. Pradhan, B. Mildenhall, P. P. Srinivasan, J. T. Barron, and H. Kretzschmar. Block-nerf: Scalable large scene neural view synthesis. In *CVPR*, 2022. 2
- [94] M. Tancik, B. Mildenhall, T. Wang, D. Schmidt, P. P. Srinivasan, J. T. Barron, and R. Ng. Learned initializations for optimizing coordinate-based neural representations. In *CVPR*, pp. 2846–2855, 2021. 2
- [95] A. Tewari, J. Thies, B. Mildenhall, P. Srinivasan, E. Tretschk, W. Yifan, C. Lassner, V. Sitzmann, R. Martin-Brualla, S. Lombardi, T. Simon, C. Theobalt, M. Nießner, J. T. Barron, G. Wetzstein, M. Zollhöfer, and V. Golyanik. Advances in Neural Rendering. *EG STAR*, 2022. doi: 10.1111/cgf.14507 2
- [96] J. Thies, M. Zollhöfer, and M. Nießner. Deferred neural rendering: Image synthesis using neural textures. *ACM TOG*, 2019. 2
- [97] H. Turki, D. Ramanan, and M. Satyanarayanan. Mega-nerf: Scalable construction of large-scale nerfs for virtual fly-throughs. In *CVPR*, pp. 12922–12931, 2022. 2
- [98] O. T. Tursun, E. Arabadzhyska-Koleva, M. Wernikowski, R. Mantiuk, H.-P. Seidel, K. Myszkowski, and P. Didyk. Luminance-contrast-aware foveated rendering. *ACM Transactions on Graphics (TOG)*, 38(4):1–14, 2019. 2
- [99] L. Wang, X. Shi, and Y. Liu. Foveated rendering: A state-of-the-art survey. *Computational Visual Media*, 9(2):195–228, 2023. 2
- [100] Z. Wang, J. Wu, R. Fan, W. Ke, and L. Wang. Vprf: Visual perceptual radiance fields for foveated image synthesis. *IEEE Transactions on Visualization and Computer Graphics*, 2024. 3
- [101] M. Weier, T. Roth, A. Hinkenjann, and P. Slusallek. Foveated Depth-of-Field Filtering in Head-Mounted Displays. *ACM Transactions on Applied Perception (TAP)*, 15(4):26, 2018. 2
- [102] M. Weier, T. Roth, E. Kruijff, A. Hinkenjann, A. Pérard-Gayot, P. Slusallek, and Y. Li. Foveated Real-Time Ray Tracing for Head-Mounted Displays. In *Computer Graphics Forum*, vol. 35, pp. 289–298. Wiley Online Library, 2016. 1, 2
- [103] M. Weier, M. Stengel, T. Roth, P. Didyk, E. Eisemann, M. Eisemann, S. Grogoric, A. Hinkenjann, E. Kruijff, M. Magnor, et al. Perception-Driven Accelerated Rendering. In *Computer Graphics Forum*, vol. 36, pp. 611–643. Wiley Online Library, 2017. 1, 2
- [104] T. Whelan, R. F. Salas-Moreno, B. Glocker, A. J. Davison, and S. Leutenegger. Elasticfusion: Real-time dense slam and light source estimation. *The International Journal of Robotics Research*, 35(14):1697–1716, 2016. 2
- [105] O. Wiles, G. Gkioxari, R. Szeliski, and J. Johnson. Synsin: End-to-end view synthesis from a single image. In *CVPR*, 2020. doi: 10.1109/CVPR42600.2020.00749 3
- [106] R. Wu, B. Mildenhall, P. Henzler, K. Park, R. Gao, D. Watson, P. P. Srinivasan, D. Verbin, J. T. Barron, B. Poole, et al. Reconfusion: 3d reconstruction with diffusion priors. In *CVPR*, pp. 21551–21561, 2024. 2
- [107] T. Wu, Y.-J. Yuan, L.-X. Zhang, J. Yang, Y.-P. Cao, L.-Q. Yan, and L. Gao. Recent advances in 3d gaussian splatting. *Computational Visual Media*, pp. 1–30, 2024. 3
- [108] Q. Xu, Z. Xu, J. Philip, S. Bi, Z. Shu, K. Sunkavalli, and U. Neumann. Point-nerf: Point-based neural radiance fields. In *CVPR*, 2022. doi: 10.1109/CVPR52688.2022.00536 3
- [109] Z. Yang, Y. Chai, D. Anguelov, Y. Zhou, P. Sun, D. Erhan, S. Rafferty, and H. Kretzschmar. Surfelgan: Synthesizing realistic sensor data for autonomous driving. In *Proceedings of the IEEE/CVF Conference on Computer Vision and Pattern Recognition (CVPR)*, June 2020. 3
- [110] Z. Yang, X. Gao, W. Zhou, S. Jiao, Y. Zhang, and X. Jin. Deformable 3d gaussians for high-fidelity monocular dynamic scene reconstruction. *arXiv preprint arXiv:2309.13101*, 2023. 3
- [111] L. Yariv, P. Hedman, C. Reiser, D. Verbin, P. P. Srinivasan, R. Szeliski, J. T. Barron, and B. Mildenhall. BakedSDF: Meshing neural SDFs for real-time view synthesis. In *SIGGRAPH, SIGGRAPH '23*. Association for Computing Machinery, 2023. doi: 10.1145/3588432.3591536 2
- [112] J. Ye, X. Meng, D. Guo, C. Shang, H. Mao, and X. Yang. Neural foveated super-resolution for real-time vr rendering. *Computer Animation and Virtual Worlds*, 35(4):e2287, 2024. 2
- [113] Z. Ye, W. Li, S. Liu, P. Qiao, and Y. Dou. Absgs: Recovering fine details for 3d gaussian splatting, 2024. 4
- [114] W. Yifan, F. Serena, S. Wu, C. Öztireli, and O. Sorkine-Hornung. Differentiable surface splatting for point-based geometry processing. *ACM TOG*, 38(6):1–14, 2019. 3
- [115] A. Yu, R. Li, M. Tancik, H. Li, R. Ng, and A. Kanazawa. PlenOctrees for real-time rendering of neural radiance fields. In *ICCV*, 2021. doi: 10.1109/ICCV48922.2021.00570 2
- [116] A. Yu, V. Ye, M. Tancik, and A. Kanazawa. pixelNeRF: Neural radiance fields from one or few images. In *CVPR*, pp. 4578–4587, 2021. doi: 10.1109/CVPR46437.2021.00455 2
- [117] Z. Yu, A. Chen, B. Huang, T. Sattler, and A. Geiger. Mip-splatting: Alias-free 3d gaussian splatting. In *Proceedings of the IEEE/CVF Conference on Computer Vision and Pattern Recognition*, pp. 19447–19456, 2024. 3
- [118] Q. Zhang, S.-H. Baek, S. Rusinkiewicz, and F. Heide. Differentiable point-based radiance fields for efficient view synthesis. *arXiv preprint arXiv:2205.14330*, 2022. 3
- [119] R. Zhang, P. Isola, A. A. Efros, E. Shechtman, and O. Wang. The unreasonable effectiveness of deep features as a perceptual metric. In *CVPR*, 2018. doi: 10.1109/CVPR.2018.00068 6
- [120] Q. Zhu, Z. Wei, Z. Zheng, Y. Zhan, Z. Yao, J. Zhang, K. Wu, and Y. Zheng. Rpbg: Towards robust neural point-based graphics in the

wild. *arXiv preprint arXiv:2405.05663*, 2024. 3

- [121] Y. Zuo and J. Deng. View synthesis with sculpted neural points. In *ICLR*, vol. abs/2205.05869, 2023. doi: 10.48550/arXiv.2205.05869  
4, 6
- [122] M. Zwicker, H. Pfister, J. Van Baar, and M. Gross. Surface splatting. In *Proceedings of the 28th annual conference on Computer graphics and interactive techniques*, pp. 371–378, 2001. 3